Mon. Not. R. Astron. Soc. **000**, 1–14 (2010) Printed 12 October 2010 (MN LATEX style file v2.2)

Debris discs in the 27 Myr old open cluster IC4665

R. Smith⋆ and R. D. Jeffries and J. M. Oliveira
Astrophysics Group, Lennard-Jones Laboratories, Keele University, Keele, Staffordshire, ST5 5BG

Accepted October 2010

ABSTRACT
We present Spitzer IRAC and MIPS 24μm imaging of members of the 27±5Myr old open cluster IC 4665. Models for the assembly of terrestrial planets through planetesimal collisions and mergers predict episodic dust debris discs at this epoch. We determine that 42^{+18}_{-13}% of the solar-type (F5-K5) cluster members have excess emission at 24μm indicative of these debris discs, the highest frequency of the clusters studied with Spitzer to date. The majority of these discs have intermediate levels of excess ($F_{24}/F_{\rm phot} < 2$), and no source is found to have extreme levels of excess indicative of a recent transient event as opposed to steady-state collisional evolution. We find no evidence of a link between multiplicity and 24μm excess in this cluster sample. Only the early-type star TYC424-473-1 ($T_{\rm eff} \sim 8420K$) has significant near-infrared excess from 4.5μm as measured with IRAC. Two solar-type targets have low significance 8μm excess but no significant 24μm excess. All other targets show no evidence for near-infrared excess which could indicate the presence of an optically thick primordial disc, demonstrating that the observed 24μm excess arises from a debris disc.

Key words: circumstellar matter – infrared: stars.

1 INTRODUCTION

A key question in astronomy today is whether the Solar System's architecture is a typical outcome of planet formation processes. Integral to this question is whether Earth-like planets exist in other systems. However, the direct detection of terrestrial planets is difficult due to the limitations of current planet detection techniques. An alternative method for determining how the planet formation process proceeds around other stars is through observation of the remnants of these processes.

Current models of planet formation propose that dusty discs around a new star settle and km-sized planetesimals aggregate on a short (<1Myr) timescale (Weidenschilling & Cuzzi 1993). The largest planetestimals undergo runaway accretion followed by oligarchic growth resulting in tens or hundreds of 1000km-sized bodies in their own cleared "feeding zones" (Klahr 2008). These phases may take up to a few million years. Finally these planetary embryos collide and merge in a chaotic growth phase to form a few stable terrestrial planets over 10-100Myr (see e.g. Weidenschilling 1977). Collisions between planetesimals produce second generation dust populations that absorb and re-radiate star light at wavelengths >10μm. In the absence of gas the lifetime of such dust is short (<1Myr, see e.g. Backman & Paresce 1993) due to collisional destruction, stellar wind drag and radiation pressure forces (Poynting-Robertson drag). The presence of a mid-infrared excess thus indicates a transient source or continuous replenishment of the dust population, a natural consequence of the ongoing growth and development of planetary systems.

The MIPS instrument on the *Spitzer Space Telescope* allows the detection of 24μm excess in nearby, young stars. Excesses detected at 24μm imply a temperature of 100-150K. Assuming thermal equilibrium this translates to an offset of 3-30AU around A and early F-type stars and 0.5-3AU in F5-K5-type stars (hereafter known as "solar-type stars"). These regions are precisely those in which we may expect to find planets.

Recent studies with Spitzer have explored the evolution of 24μm excess in a statistical manner (see e.g. Rieke et al. 2005, Su et al. 2006, Siegler et al. 2007, Rebull et al. 2008, Carpenter et al. 2009). These studies have tried to answer the question of why two apparently similar stars can have very different levels of excess emission. To date, the clearest dependency is on age. In A and early F-type stars there is evidence for a peak in the upper envelope of excess emission at 10-20Myr before a decay in proportion with time (see e.g. Wyatt 2008 and references therein). For solar-type stars the number of observed objects is smaller and so correlations are harder to establish. Based on current evidence the decay of 24μm excess around solar-type stars appears to follow a similar pattern to the A stars but on a timescale that is an order of magnitude shorter (drop from 40% to 20% of stars with 24μm excess occurs from 10-100Myr for solar-type

⋆ E-mail: rs@astro.keele.ac.uk

stars, and from 100-500Myr for A-type stars, see Figure 6 of Siegler et al. 2007). In general the levels of excess emission are also smaller around lower mass objects (<2 times the photosphere) apart from around the youngest sources. These results can be interpreted within the framework of the evolutionary models of Kenyon and Bromley (2005; 2006). These suggest that planetesimals take longer to form at 10-30AU around A-type stars than at ∼1AU around G-type stars, and thus there are copious dust producing collisional events for 10-100Myr during planetesimal accretion. Around solar-type stars 100km-sized embryos may be complete within a few Myr, and thus subsequent observed debris is likely to have been produced in recent catastrophic collisions like the impact that formed the Earth-Moon system (see e.g. Canup 2004 and references therein).

Within this framework we would expect to find small or no excess emission around most solar-type stars with occasional high excess resulting from a recent massive collision in the terrestrial planet zone (evidence for an Earth-Moon type collision has been presented around the ∼12Myr old star HD172555, Lisse et al. 2009). The majority of these collisions are expected in the age range 10-50Myr (see e.g. Chambers 2001). The distribution of excess depends on the frequency of impacts and the timescale for removal of the resulting dust from the system, which is in turn dependent on the dust particle size distribution.

In this paper we present a study of the debris disc population of the open cluster IC 4665 (370±50pc Mamjek 2007). The cluster has reddening of $E(B-V) = 0.18 \pm 0.05$mag (Hogg & Kron 1955; Crawford & Barnes 1972 - corresponding to $E(V-I) = 0.23 \pm 0.06$ and $A_{\rm V} = 0.59 \pm 0.16$ for the intrinsic colours of a low mass PMS star, Bessell et al. 1998). Open clusters provide a homogeneous, chemically uniform coeval population for which debris disc incidence rates can be calculated. IC 4665 is one of only 5 clusters to have an age measured using the lithium depletion boundary giving a more accurate age determination than from H-R diagram analysis. The determined age of 27±5 Myr (Manzi et al. 2008) makes it a prime target for studying the debris disc population during the period of terrestrial planet formation.

In this paper we describe Spitzer IRAC and MIPS 24μm photometry of confirmed members of IC 4665. We determine those stars with excess 24μm emission based on their position in a $K_s - 24$ vs. $V - K_s$ colour-colour diagram and on SED fitting. We discuss how the rates and levels of excess emission compare with other studies of solar-type stars and how these observations constrain models of terrestrial planet formation.

2 IC 4665 TARGETS

Our primary aim in this study is to determine the disc population in the solar-type stars in IC 4665. We base our sample on the study by Jeffries et al. (2009) who used fibre spectroscopy to establish cluster membership from a sample of 452 photometric candidates. Membership was assessed primarily from radial velocity, giving a candidate list of 56 stars. This was further refined through measurements of Ca I lines at 6439 and 6463Å to filter out contamination by K-giants. Mean proper motions for 45 of the candidate stars (taken from the NOMAD database, Zacharias et al. 2005) are -0.7 ± 1.0 mas yr^{-1} in RA and -6.2 ± 0.8 mas yr^{-1} in Dec. Two stars were found to have proper motions incompatible with cluster membership at the 3σ level. A final sample of 40 candidates were confirmed as low mass cluster members. For these targets we used the 2MASS catalogue (Skrutskie et al. 2006) to determine the K_s band magnitude of the targets. Temperatures were taken from Jeffries et al. (2009). These sources are listed in Table 1.

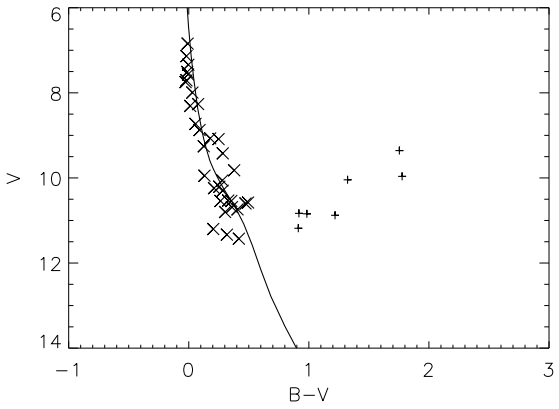

Figure 1. A V vs $B-V$ colour-magnitude diagram of bright candidate members of IC 4665 from Tycho. Here we show only sources with proper motions consistent with cluster membership. Those sources with colours consistent with membership are marked by large crosses. Overplotted is a 30Myr isochrone from Siess et al. (2000) is shown with conversion following Kenyon & Hartmann (1995), adjusted for a distance of 370pc, A_V=0.59mag and $E(B-V)$=0.18.

To complement the low mass sample we searched the Tycho catalogue (Høg et al. 2000) for higher mass candidate members within a 1 degree radius of the center of our Spitzer observations at RA17$^{\rm h}$46$^{\rm m}$16$^{\rm s}$.0, Dec5°41′53″ (see section 3 for details of the observed region). A candidate list of 132 stars with 6 < V < 12 were selected. This list was refined firstly by excluding candidates with proper motions incompatible with the mean cluster proper motion (at the 3σ level as determined by Jeffries et al. 2009). This reduced the candidate high mass population to 41 stars. This list was further reduced by examination of the source colours in a $B-V$ vs V colour-magnitude diagram (Figure 1). We adopt a 30Myr old isochrone from Siess et al. (2000). Seven stars are found to have colours incompatible with cluster membership, and our final list of additional bright targets comprises of 33 members. We further add to our list the solar-type targets P39 and P155 from the study of IC 4665 by Prosser & Giampapa (1994). These targets were identified as possible members based on their radial velocities and were not excluded by Jeffries et al. (2009) but not observed by them spectroscopically. Temperatures for these sources were determined from the B and V magnitudes of the star

$$B - V = -3.684 \log T_{\rm eff} + 14.551.$$

Our final list of additional targets and their parameters is given in Table 2.

Identifier	RA	Dec	V	$V-K_s$	$T_{\rm eff}$, K
JCO1_427	266.814	5.94327	13.0690	2.200	5742
JCO1_530	266.885	5.87545	12.5180	1.655	6389
JCO2_145	266.631	6.09112	12.2720	1.638	6450
JCO2_213	266.483	6.04839	13.2180	2.037	6062
JCO2_220	266.599	6.04287	16.4200	4.079	3856
JCO2_373	266.530	5.93018	12.4560	2.019	6214
JCO2_637	266.662	6.03693	17.2000	4.936	3456
JCO3_065	266.379	6.11816	15.0450	3.377	4375
JCO3_285	266.149	5.95576	13.3360	1.721	6340
JCO3_357	266.112	5.90146	13.5170	2.476	5128
JCO3_395	266.354	5.86076	13.7160	2.280	5426
JCO3_396	266.242	5.85915	13.4260	2.086	5758
JCO3_770	266.112	5.86267	17.5610	5.105	3470
JCO4_053	267.021	5.81170	13.5280	2.663	5071
JCO4_226	266.899	5.64882	13.7810	2.359	5730
JCO4_337	266.954	5.54434	13.9130	3.052	4584
JCO4_437	266.735	5.79573	16.7160	4.364	3806
JCO4_459	266.833	5.78159	17.8930	4.866	3488
JCO4_591	266.876	5.68092	16.2360	3.912	4007
JCO5_179	266.550	5.69051	14.4070	2.840	4900
JCO5_280	266.471	5.60814	14.2430	2.479	5166
JCO5_282	266.412	5.60645	12.1460	1.626	6608
JCO5_296	266.603	5.59392	13.9400	2.447	5243
JCO5_472	266.579	5.77233	16.9100	4.260	3738
JCO5_515	266.671	5.73845	17.8510	5.045	3458
JCO5_521	266.444	5.73190	17.0620	4.527	3638
JCO6_088	266.331	5.79448	13.7160	2.233	5587
JCO6_095	266.113	5.78877	13.5110	2.244	5668
JCO6_111	266.333	5.77487	15.9930	3.745	4120
JCO6_240	266.171	5.69883	11.6580	1.214	7418
JCO7_021	266.889	5.52944	13.1260	2.316	5635
JCO7_079	266.826	5.50173	13.0880	1.929	6286
JCO7_088	266.818	5.49708	15.4110	3.971	4001
JCO7_670	266.935	5.36262	17.3490	5.028	3489
JCO8_257	266.603	5.28927	12.9210	2.109	5459
JCO8_364	266.648	5.51877	17.5300	4.847	3478
JCO8_395	266.394	5.49829	17.6510	4.710	3507
JCO8_550	266.694	5.37568	17.8720	5.340	3430
JCO9_120	266.203	5.48869	14.4050	2.414	5132
JCO9_281	266.364	5.40240	14.9560	3.096	4521

Table 1. Target sources in this study. These sources, taken from Jeffries et al. (2009), are confirmed members of IC 4665.

Identifier	RA	Dec	V	$V-K_s$	$T_{\rm eff}$, K
TYC424-75-1	266.838	5.59961	10.739	0.974	6910
TYC428-1339-1	266.759	5.69184	7.993	0.127	8740
TYC428-1483-1	266.762	5.69863	10.059	0.579	7480
TYC424-55-1	266.695	5.56493	8.263	0.402	8483
TYC428-969-1	266.840	5.75952	9.947	0.772	8208
TYC424-473-1	266.741	5.42569	8.874	0.410	8420
TYC428-737-1	266.671	5.77427	7.137	0.074	9017
TYC428-1685-1	266.546	5.65822	7.339	0.046	8927
TYC424-1087-1	266.531	5.53021	6.843	0.025	8960
TYC428-1300-1	267.181	5.70126	7.508	-0.011	8979
TYC428-1571-1	266.488	5.69444	7.567	-0.020	8941
TYC424-174-1	266.786	5.22533	10.686	0.899	7115
TYC424-292-1	266.969	5.23321	11.478	1.464	6863
TYC428-1938-1	266.485	5.81237	11.200	1.253	7842
TYC428-1755-1	266.579	5.93536	10.601	1.112	6630
TYC428-675-1	266.390	5.71569	7.707	0.131	9013
TYC424-309-1	266.395	5.42651	9.087	0.715	7628
TYC428-691-1	266.539	5.98235	10.531	0.939	7253
TYC424-223-1	266.913	5.11635	10.240	0.780	7808
TYC428-1910-1	266.322	5.66767	9.070	0.513	7968
TYC428-215-1	266.652	6.12062	7.748	-0.041	9056
TYC424-1396-1	266.415	5.19808	9.820	1.000	7032
TYC424-128-1	266.254	5.52291	9.422	0.840	7464
TYC424-256-1	267.373	5.24004	10.299	1.020	7468
TYC428-1445-1	267.424	5.92507	10.800	0.974	7373
TYC428-1211-1	266.945	6.29000	10.578	0.570	6542
TYC428-847-1	267.043	6.27151	9.256	0.434	8239
TYC428-840-1	266.838	6.37147	11.333	0.462	7303
TYC427-1623-1	266.066	5.71430	8.308	0.266	8842
TYC423-66-1	265.983	5.41341	10.205	0.570	7596
TYC423-369-1	265.958	5.42050	8.730	0.260	8601
TYC427-1661-1	266.175	6.23509	10.541	0.706	7551
TYC428-1933-1	266.275	6.36365	10.541	1.177	7138
P39	266.609	5.82858	12.9300	2.011	5574
P155	266.934	5.36664	13.5200	2.294	5043

Table 2. Target sources in this study. These targets from Tycho and Prosser (P39 and P155) are likely members of IC 4665 based on proper motion and colour. See text for details.

3 SPITZER DATA

Data were obtained with the Spitzer Space Telescope IRAC (Fazio et al. 2004) and MIPS (Rieke et al. 2004) instruments under Spitzer Program P40601. MIPS data were obtained in scan mapping mode centered on the cluster centre of 17h46m16s +5d41′53″. A medium scan rate, scan leg length of 0.5° and 20 scan legs were used to cover an area of 50′× 50′with an exposure of ∼80s at each sky position were used in each AOR. This AOR was performed four times to achieve the required sensitivity.

For IRAC the observations followed the Spitzer observing manual instructions for a rapid shallow survey. A 12 × 12 mapping array was used to cover a similar area to the MIPS survey. The AOR used 280″ map steps, array orientation and a 3-point cycling dither with medium scale factor. High dynamic range mode with 12 second exposures gave an effective on-sky exposure of 36 seconds and avoids saturation in the range $7 < K < 13$.

The data were extracted as BCD (basic calibrated data) files from the Spitzer archive. These data are individually flux-calibrated array images. The Spitzer Science Center MOPEX package (Makovoz & Marleau 2005) was used to produce the final mosaics. We used standard MOPEX modules. The individual 24μm MIPS frames were flat-fielded using the flatfield module in MOPEX. Overlap correction was determined using the default settings in the overlap module and the final image mosaic consisting of all four repetitions of the AOR was constructed using the mosaic module. Mosaics were created for each of the IRAC channels using the overlap and mosaic modules in MOPEX under default settings. For details of these modules see Makovoz & Marleau (2005) or the on-line MOPEX user's guide at http://ssc.spitzer.caltech.edu/dataanalysistools/tools/mopex/mopexusersguide/.

Photometry was extracted using the APEX package from MOPEX. For the IRAC channels the PSF is undersampled and thus photometry was extracted in a circular aperture of radius 3 pixels (∼3.″6) with background determined in an annulus of inner radius 12 pixels and outer

radius 20 pixels ($\sim$14.″4 – 24″). Apertures were centered on the location of each source as listed in Tables 1 and 2. Of the targets in Table 2, 12 fell outside the image mosaics. Photometry was corrected for the array-location using correction images available online. These correction images were mosaiced in the same way as the data frames to produce a correction mosaic as described in the IRAC data handbook. Aperture corrections were taken from tabulated values in the data handbook. Colour corrections were applied by interpolation from tabulated values using the effective temperatures listed in Tables 1 and 2. We used the tabulated values in the IRAC data handbook to convert the flux in Jy to magnitude. Specifically, the zero points used were 280.9Jy at 3.6μm, 179.7Jy at 4.5μm, 115.0Jy at 5.8μm, and 64.1Jy at 8μm. Absolute calibration of IRAC is stable to 1–3% (Reach et al. 2005). We add this 3% error in quadrature to statistical background errors determined from pixel to pixel variation in the aperture module to give a final error on the IRAC photometry. The final photometry is listed in Table 3.

For the MIPS data the PSF is not undersampled. We used the APEX PRF(Point Response Function) fitting module to determine a PRF model for the final mosaic. As the PRF can vary for source colour we grouped the list of targets by $V-K_s$ magnitude (from 0-6 for our targets, grouped so $\delta(V-K_s)$=1) and used the brightest and cleanest (no near neighbours, no bad pixels) sources in each group as the basis for the PRF model. The prf_estimate module was used to determine the PRF models for each source. These models were used to fit the target stars to determine the source position and flux in the PRF photometry module in APEX. If the source could not be well fit (according to a χ^2 analysis) with either a single or multiple point sources (active deblend), then the PRF photometry was determined to have failed. For sources which were not fit in the PRF photometry, or where these fits were sufficiently distant (>1.″225 corresponding to 1/5 the FWHM of the average PSF for all sources) from the input source position that the detected source was unlikely to be our target, then aperture photometry was adopted instead. Apertures of radius 2.6 pixels (6.″37) were used with annuli of inner radius 8.16 pixels and outer radius 13.06 pixels (20″– 32″) to determine the background.

Some of our target stars are close enough to other objects for contamination of aperture photometry to become an issue. To determine a correction for contaminating sources we used the APEX module in MOPEX to create a list of all source detections ($>3\sigma$) in the MIPS 24μm image. We determined the sources that were most isolated (no other detection within > 10 pixels, 24.″5 of the target) and grouped them by brightness (PRF determined flux). We then used the aperture module to place apertures at the source and at increasing distance from the source (in a direction away from other sources) to determine the level of flux that would fall into an aperture at a set distance from the source. These profiles were found to be well fit by a Gaussian profile with FWHM of 8.″7 (3.5 pixels). Flux from the target was <5% of the flux measured in an on-source aperture at >13.″5 and <1% of the on-source flux at >16.″9. For each of our target sources the area within 20″was checked for detected sources in the 24μm image, and any possible contamination calculated by multiplying the aperture flux by the value of the Gaussian function described above at appropriate distance. In order to account for the possibility that sources below the 3σ detection threshold may be contaminating the source we also considered the detections recorded by the APEX module in the IRAC 8μm image. The relation between 8μm and 24μm flux was calculated by comparing the values determined for sources detected in both images. The median and median absolute deviation for the ratio of measured fluxes was $F_{8\mu\mathrm{m}}/F_{24\mu\mathrm{m}} = 1.32\pm0.856$. Any sources within 20″of our target detected at 24μm had their contamination included, the source was removed from the list of detected sources at 8μm and then the 8μm list of detections was checked for any additional sources within 20″. The flux of these sources was divided by 1.32 to get a 24μm flux and the contamination in the aperture around our target calculated as above. The median and median absolute deviation of the contamination for our targets is 3% ± 3% of the aperture flux. Sources with high levels of contamination or other issues (e.g. close to edge of array) are noted in Table 3. PRF photometry should mitigate against the effects of nearby contaminants through the active deblend algorithm. We used the above steps to determine the levels of contamination that would be seen in aperture photometry for those sources with PRF photometry. This was used as a method for checking that there were no nearby sources in the IRAC 8μm mosaic that could have been blended with the target source in the MIPS 24μm mosaic (as this has lower resolution). In all cases the possible contamination was $\leqslant$1.5% the PRF photometry.

After subtracting the contaminating flux an aperture correction of 0.729 magnitudes determined from bright targets was applied. A colour correction was applied for each source by interpolation from values tabulated in the MIPS data handbook. We used the zero point of 7.14Jy listed in the handbook to convert the fluxes into magnitudes. Photometric error for MIPS 24μm observations is 4% (Engelbracht et al. 2007). We add this in quadrature to statistical error returned from the aperture/APEX PRF photometry modules arising from pixel to pixel variations to give a final error on the flux. The final MIPS photometry is listed in Table 3. For 4 of our targets (JC04_053, TYC424-174-1 TYC424-292-1 and TYC424-1396-1) the source falls outside the MIPS 24μm mosaic and therefore it is not listed in Table 3.

4 DETERMINATION OF 24μM EXCESS

We follow the example of recent authors (Rebull et al. 2008; Stauffer et al. 2010) in using the $K_s-[24]$ colour of our sources to determine which of our targets exhibits 24μm excess emission. This requires a well defined model for photospheric colours. Recently Stauffer et al. (2010) used Spitzer observations of the Hyades cluster to determine an empirical relation for K_s - [24] from $V-K_s$, defined as $K_s-[24] = 0.042 - 0.053\times(V-K_s) + 0.023\times(V-K_s)^2$. They found that this relation was very similar to that proposed by Gorlova et al. (2006), but differed from the relation given by Plavchan et al. (2009) that included M dwarf stars. The Stauffer et al. relation is only valid for sources with $V-K_s<3$.

In Figure 2 we show the $K_s-[24]$ vs $V-K_s$ colours

Table 3. Spitzer IRAC and MIPS 24μm data on confirmed or suspected members of IC 4665.

Source	[3.6]	[4.5]	[5.8]	[8.0]	[24]	$K_s - [24]$	$F_{24}/F_{\rm phot}$	Comments
JCO1_427	10.802 [0.033]	10.823 [0.033]	10.804 [0.034]	10.806 [0.035]	10.725 [0.100]	0.144	1.093	
JCO1_530	10.877 [0.033]	10.860 [0.033]	10.849 [0.034]	10.890 [0.035]	11.060 [0.200]^l	-0.197^l	0.808^l	Edge
JCO2_145	10.615 [0.033]	10.602 [0.033]	10.608 [0.033]	10.612 [0.034]	10.458 [0.106]	0.176	1.139	
JCO2_213	11.147 [0.033]	11.165 [0.033]	11.134 [0.034]	11.207 [0.036]	10.802 [0.174]	0.379	1.374	XS
JCO2_220	12.227 [0.033]	12.225 [0.034]	12.194 [0.036]	12.253 [0.051]	12.092 [0.667]^l	0.249^l	0.925^l	
JCO2_373	10.363 [0.033]	10.349 [0.033]	10.324 [0.034]	10.348 [0.034]	9.882 [0.085]	0.555	1.616	XS
JCO2_637	11.821 [0.034]	11.793 [0.033]	11.786 [0.034]	11.731 [0.042]	11.551 [0.326]^l	0.713^l	1.338^l	
JCO3_065	11.815 [0.033]	11.568 [0.033]	11.548 [0.038]	11.546 [0.038]	11.234 [0.318]	0.434	1.210	
JCO3_285	11.569 [0.033]	11.569 [0.033]	11.569 [0.035]	11.717 [0.041]	11.827 [0.454]^l	-0.212^l	0.797^l	Contam.
JCO3_357	10.972 [0.033]	10.954 [0.033]	10.814 [0.034]	10.889 [0.035]	10.898 [0.112]	0.143	1.058	
JCO3_395	11.443 [0.033]	11.412 [0.033]	11.433 [0.035]	11.425 [0.038]	11.049 [0.122]	0.387	1.354	XS
JCO3_396	11.281 [0.033]	11.277 [0.033]	11.265 [0.034]	11.261 [0.035]	10.784 [0.104]	0.556	1.616	XS
JCO3_770	12.210 [0.034]	12.205 [0.034]	12.133 [0.036]	12.148 [0.049]	12.450 [0.935]^l	0.006^l	0.691^l	
JCO4_226	11.462 [0.033]	11.377 [0.033]	11.397 [0.035]	11.390 [0.038]	12.114 [0.605]^l	-0.692^l	0.497^l	Contam.
JCO4_337	10.780 [0.033]	10.902 [0.033]	10.753 [0.034]	10.721 [0.034]	11.817 [0.483]^l	-0.956^l	0.351^l	Contam.
JCO4_437	12.228 [0.033]	12.200 [0.034]	12.160 [0.036]	12.148 [0.049]	11.523 [0.312]	0.829	1.545	
JCO4_459	12.740 [0.034]	12.730 [0.034]	12.676 [0.040]	12.668 [0.064]	11.911 [0.479]^l	1.116^l	1.948^l	
JCO4_591	12.249 [0.033]	12.307 [0.033]	12.256 [0.037]	12.246 [0.045]	11.797 [0.442]^l	0.527	1.229	
JCO5_179	11.415 [0.033]	11.431 [0.033]	11.424 [0.035]	11.421 [0.036]	11.511 [0.342]^l	0.056^l	0.926 ^{l}	
JCO5_280	11.711 [0.033]	11.756 [0.033]	11.771 [0.035]	11.750 [0.042]	11.859 [0.451]^l	-0.095^l	0.850^l	Contam.
JCO5_282	10.518 [0.033]	10.532 [0.033]	10.528 [0.034]	10.532 [0.034]	10.221 [0.104]	0.299	1.276	XS
JCO5_296	11.368 [0.033]	11.459 [0.033]	11.305 [0.034]	11.336 [0.038]	10.688 [0.152]	0.805	1.952	XS
JCO5_472	12.386 [0.034]	12.411 [0.034]	12.348 [0.038]	11.957 [0.044]	11.596 [0.343]^l	1.054^l	1.914^l	
JCO5_515	12.505 [0.033]	12.465 [0.034]	12.377 [0.038]	12.515 [0.054]	11.647 [0.378]^l	1.159^l	2.005^l	
JCO5_521	12.318 [0.034]	12.281 [0.034]	12.336 [0.040]	12.293 [0.053]	11.808 [0.446]^l	0.727^l	1.389^l	
JCO6_088	11.414 [0.033]	11.423 [0.033]	11.386 [0.034]	11.442 [0.036]	10.895 [0.115]	0.588	1.638	XS
JCO6_095	11.240 [0.033]	11.239 [0.033]	11.236 [0.034]	11.251 [0.037]	11.248 [0.260]	0.019	0.968	
JCO6_111	12.132 [0.033]	12.156 [0.033]	12.077 [0.036]	12.048 [0.040]	11.755 [0.433]^l	0.493^l	1.223^l	Contam.
JCO6_240	10.410 [0.033]	10.403 [0.033]	10.282 [0.033]	10.431 [0.034]	9.650 [0.076]	0.794	2.014	XS
JCO7_021	10.688 [0.033]	10.686 [0.033]	10.676 [0.034]	10.717 [0.034]	10.675 [0.100]	0.135	1.069	
JCO7_079	11.106 [0.033]	11.091 [0.033]	11.095 [0.034]	11.109 [0.036]	10.658 [0.146]	0.501	1.537	XS
JCO7_088	11.257 [0.033]	11.269 [0.033]	11.252 [0.035]	11.230 [0.037]	11.120 [0.222]	0.320	1.005	
JCO7_670	12.068 [0.033]	12.053 [0.033]	11.812 [0.036]	12.043 [0.044]	–	-	–	Edge
JCO8_257	10.691 [0.033]	10.699 [0.033]	10.684 [0.034]	10.722 [0.035]	9.857 [0.143]	0.955	2.331	XS
JCO8_364	12.465 [0.034]	12.449 [0.033]	12.337 [0.038]	12.337 [0.043]	12.383 [0.883]^l	0.300^l	0.920^l	
JCO8_395	12.665 [0.034]	12.656 [0.034]	12.567 [0.040]	12.614 [0.065]	14.234 [0.853]^l	-1.293^l	0.214^l	
JCO8_550	12.297 [0.033]	12.246 [0.034]	12.210 [0.037]	12.230 [0.051]	12.183 [0.749]^l	0.349^l	0.935^l	
JCO9_120	11.999 [0.033]	12.062 [0.034]	12.038 [0.036]	12.012 [0.046]	11.645 [0.379]^l	0.346^l	1.285^l	
JCO9_281	11.740 [0.033]	11.808 [0.034]	11.742 [0.035]	11.765 [0.042]	12.332 [0.836]^l	-0.472	0.543	
TYC424-75-1	9.855 [0.034]	9.734 [0.033]	9.643 [0.034]	9.777 [0.034]	9.677 [0.074]	0.088	1.050	
TYC428-1339-1	8.444 [0.033]*	7.989 [0.032]*	7.942 [0.032]	7.976 [0.032]	7.563 [0.056]	0.303	1.280	XS
TYC428-1483-1	9.450 [0.033]	9.442 [0.032]	9.454 [0.032]	9.480 [0.032]	9.392 [0.067]	0.088	1.051	
TYC424-55-1	8.435 [0.033]*	8.085 [0.032]*	7.892 [0.032]	7.937 [0.032]	7.756 [0.056]	0.106	1.069	
TYC428-969-1	9.189 [0.033]	9.126 [0.032]	9.139 [0.032]	9.174 [0.032]	8.817 [0.059]	0.358	1.347	XS
TYC424-473-1	8.686 [0.033]*	8.456 [0.032]	8.144 [0.032]	7.952 [0.032]	6.641 [0.056]	1.823	5.193	XS
TYC428-737-1	9.189 [0.033]*	8.389 [0.032]*	7.122 [0.032]	7.166 [0.032]	7.254 [0.056]*	-0.191*	0.813*	
TYC428-1685-1	9.383 [0.033]*	7.716 [0.032]*	7.360 [0.032]	7.386 [0.032]	7.315 [0.056]	-0.022	0.952	
TYC424-1087-1	8.918 [0.033]*	8.613 [0.032]*	6.901 [0.032]	6.962 [0.032]	7.069 [0.056]*	-0.252*	0.768*	
TYC428-1571-1	9.550 [0.033]*	7.907 [0.032]*	7.639 [0.032]	7.703 [0.032]	7.648 [0.056]	-0.061	0.916	
TYC428-1938-1	9.897 [0.033]	9.862 [0.032]	9.887 [0.032]	9.923 [0.032]	9.213 [0.066]	0.734	1.904	XS
TYC428-1755-1	9.456 [0.033]	9.433 [0.032]	9.447 [0.032]	9.474 [0.032]	9.244 [0.065]	0.245	1.219	XS
TYC428-675-1	8.885 [0.033]*	8.026 [0.032]*	7.666 [0.032]	7.695 [0.032]	7.756 [0.056]	-0.180	0.821	
TYC424-309-1	8.669 [0.033]*	8.391 [0.032]	8.367 [0.032]	8.421 [0.032]	8.351 [0.057]	0.021	0.988	
TYC428-691-1	9.573 [0.033]	9.564 [0.032]	9.575 [0.032]	9.617 [0.032]	9.583 [0.071]	0.009	0.977	
TYC428-1910-1	8.833 [0.033]*	8.565 [0.033]	8.563 [0.033]	8.608 [0.033]	8.512 [0.058]	0.045	1.010	
TYC428-215-1	8.391 [0.088]	8.060 [0.032]*	7.816 [0.034]	7.918 [0.032]	7.918 [0.056]	-0.129	0.860	
TYC424-128-1	8.864 [0.033]*	8.744 [0.032]*	8.601 [0.032]	8.650 [0.032]	8.296 [0.057]	0.286	1.261	XS
P39	10.860 [0.033]	10.788 [0.032]	10.787 [0.032]	10.833 [0.032]	10.516 [0.137]	0.403	1.404	XS
P155	11.124 [0.033]	11.130 [0.032]	11.116 [0.032]	10.953 [0.032]	–	–	–	Edge

* = Saturated photometry. ^{l} = Signal to noise < 5. XS = Significant 24μm excess emission. Contam. = High level of contamination in 24μm photometry. Edge = Source falls on edge of 24μm mosaic.

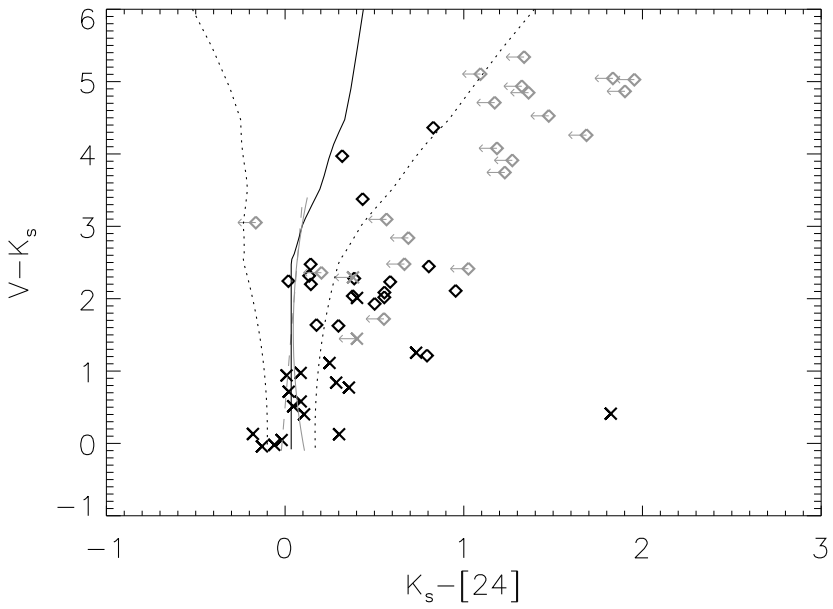

Figure 2. A colour-colour plot of the IC4665 target stars used to determine 24μm excess. The solid black line is the expected photospheric relation from Plavchan et al. (2009), with dotted black lines showing 3σ limits from errors on the 24μm photometry (see text). Also shown are the photospheric relations from Gorlova et al. (2006) (dashed grey line) and Stauffer et al. (2010) (solid grey line) which do not cover the full range of $V-K$ needed for this study. Diamond symbols show the targets taken from Jeffries et al. (2009) and crosses mark the sources listed in Table 2. Grey symbols mark the 5σ upper limits for sources with low signal to noise (<5).

of our target sources. The diamonds and crosses mark the target sources from Jeffries et al. (2009) as listed in Table 1 and the brighter targets as listed in Table 2 respectively. Colours are shown in grey as upper limits if the target has a signal to noise of less than 5σ in the 24μm photometry. Overplotted as a solid line is the expected photospheric colour from Plavchan et al. (2009). We also show the relations from Gorlova et al. (2006) (dashed grey line) and from Stauffer et al. (2010) (solid grey line). As our target sources cover the range $0 < V-K < 6$ we adopt the Plavchan et al. (2009) relation as our photospheric model. Following the example of Stauffer et al. (2010) the 3 σ errors on this relation are taken from the errors on the 24μm photometry. We used all significant ($>5\sigma$) detections to calculate a quadratic relation between error (as given in Table 3) and $V-K_s$ which was determined to be $0.045 + 0.004 \times (V-K_s) + 0.008 \times (V-K_s)^2$. The scatter around this fit is low, with a median difference between the fitted error and measured error of 2%.

From the figure we can identify 10 of the sources from Jeffries et al. (JCO2_213, JCO2_373, JCO3_395, JCO3_396, JCO5_282, JCO5_296, JCO6_088, JCO6_240, JCO7_079 and JCO8_257) and 7 of the additional targets (TYC428-1339-1, TYC428-969-1, TYC424-473-1, TYC428-1938-1, TYC428-1755-1, TYC424-128-1, P39) that have $K_s-[24]$ greater than the 3σ limit on the photospheric colours. Excluding the targets which do not fall within the MIPS 24μm mosaic (see section 3) this gives a total of 16/59 sources or 27^{+9}_{-7}%. If we consider only the sources with confirmed membership, i.e. those from Jeffries et al., we have an excess detection frequency of 10/39 or 26^{+11}_{-8}%. Note that 2 targets appear to have 3σ negative detections. These targets have very low $V-K_s$, in the range at which the models of Stauffer et al. (2010), Gorlova et al. (2006), and Plavchan et al. (2009) most differ. If we were to use the Gorlova et al. (2006) models for the photospheric colours these targets would be within 3σ of the expected colour, however this model does not cover the full $V-K_s$ range of interest in this study. Using any of the considered models does not change the conclusions regarding which sources have 24μm excess.

4.1 Near infrared excess?

In addition to the MIPS 24μm observations we have IRAC photometry across 4 channels which allows us to search for evidence of near-infrared excess. If any stars exhibit near-infrared excess we could be seeing the remnants of an optically thick primordial disc rather than a true debris disc. At the 27Myr age of this cluster such primordial discs would be rare as they are expected to dissipate on a timescale of a few Myr (see e.g. Wyatt 2008 and references therein). Transition discs would also be unexpected, as the lifetime of such discs is expected to be very short, <1Myr, (Skrutskie et al. 1990).

To determine if any excess emission exists in the IRAC photometry we plot the $K_s-[3.6]$, $K_s-[4.5]$, $K_s-[5.8]$, and $K_s-[8.0]$ colours against $V-K_s$. These plots can be seen in Figure 3. In all panels the diamonds and crosses mark the targets from Jeffries et al. (2009) and those listed in Table 2 respectively. Those sources marked with square boxes are those which are saturated in the IRAC image and therefore have very unreliable photometry in this band (these

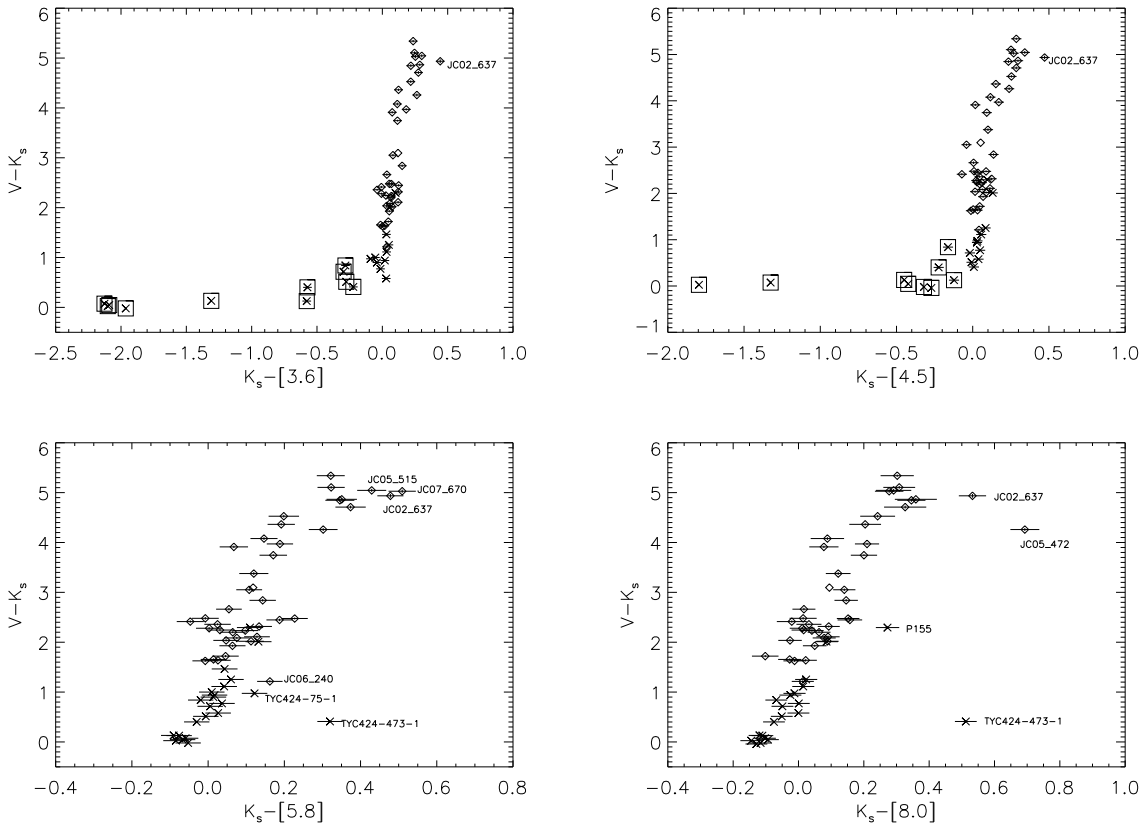

Figure 3. A colour-colour plot of the IC4665 target stars for each of the IRAC channels. Diamond symbols show the targets taken from Jeffries et al. (2009) and crosses mark the sources listed in Table 2. Sources are shown with 1σ errors from the IRAC photometry. Sources that appear saturated in the IRAC image are indicated by a surrounding square box. Labelled sources have colours that may indicate excess in this IRAC band. See text for discussion.

are marked in Table 3 with an asterisk). Overplotted are the errors from the IRAC photometry. Sources with colours that may indicate excess are labelled, and we discuss these individually below.

4.1.1 Poor K_s photometry

The source JC02_637 has apparent excess in all IRAC channels. The 2MASS catalogue record for this target from which we obtain K_s flags the JHK_s results as poor due to issues in the PSF fit photometry. Furthermore if we produce an SED fit to the temperature of the target as listed in Jeffries et al. (2009) and scaled to the IRAC 3.6μm flux the results from the remaining channels are consistent with photospheric emission alone. Thus we do not believe we have evidence for a near-infrared excess around this target. Note that as one of our coolest targets the 24μm MIPS detection of this source is below a signal to noise threshold of 5, and thus we have only upper limits on the 24μm flux.

4.1.2 Insignificant excess

Two further sources, JC05_515 and JC07_670, with similar $V - K_s$ have possible evidence for excess at 5.8μm. For targets in the range $4.5 < V - K_s < 5.5$ (excluding JC02_637, JC05_515 and JC07_670) we have an average $K_s - [5.8]$ of 0.346 ± 0.062. The colour of JC05_515 is $K_s - [5.8] = 0.429 \pm 0.048$, consistent with this range. The colour of JC07_670, $K_s - [5.8] = 0.509 \pm 0.048$ is closer to indicative of a significant excess. As there is no evidence for excess in the other IRAC bands, there is no significant evidence for a near-infrared excess which could indicate a primordial disc remnant.

The source JC06_240 also has apparent 5.8μm excess. In this case comparison with targets of similar colour (JC06_240 has $V - K_s = 1.214$, we look at targets with $0.7 < V - K_s < 1.7$) suggests we may have a significant 5.8μm excess; JC06_240 has $K_s - [5.8] = 0.162 \pm 0.040$, the average for stars of a similar colour is 0.026 ± 0.025. However, once again there is no evidence for excess in the other IRAC bands including at 8μm. This source lies on the edges of different tiles in the IRAC channel 3 imaging and pixels in the source location have a high level of standard deviation across different exposures, and so the error (taken from the Spitzer uncertainty images) is underestimated. Adopting the uncertainty from the standard deviation between exposures instead gives $K_s - [5.8] = 0.162 \pm 0.084$. Other sources in the $0.7 < V - K_s < 1.7$ spectral range were checked and none were found to have a similarly high standard deviation.

4.1.3 Contaminated IRAC photometry

The target TYC424-75-1 has an apparent excess at 5.8μm, however examination of the 5.8μm image shows that it is close to a very bright target which contaminates the 5.8μm aperture and which is responsible for the high $K_s-[5.8]$. The flux from this bright source lies just outside the apertures at 3.6 and 4.5μm, and the lower brightness at 8.0μm means that it does not spread to contaminate the flux of TYC424-75-1 in this band.

4.1.4 Significant near-infrared excess

For TYC424-473-1 the difference between this and other targets of similar colour in $V-K_s$ is highly significant. This source is also reddened in the $K_s-[5.8]$ plot. This near-infrared excess could indicate the presence of a remnant primordial disc. We construct an SED for this object using a Kurucz profile for a temperature of 8337K (Figure 4). The photospheric model is scaled to a best fit to the JHK_s 2MASS photometry using a χ^2 analysis. From this plot it is clear that the near infrared slope of the target is not consistent with photospheric emission alone unless the target has been misidentified. However, a single temperature blackbody added to the photospheric emission can be shown to fit the IRAC and MIPS data. Overplotted on the SED is a 500K blackbody emission profile (dotted line) and the total emission from this plus the photospheric profile (dashed line). This total emission profile fits the Spitzer data within the errors (note that this target is saturated in the IRAC 1 channel, and so the [3.6] data is ignored). The fractional luminosity of this fit is $f = L_{IR}/L_\star = 2.6\times10^{-3}$. This is within the range expected for debris discs ($f < 10^{-2}$, Lagrange et al. 2000) and lower than a primordial disc. Thus we can assume the dust is optically thin, and thus this temperature implies a distance of 1.7AU from the central star assuming that the emitting material behaves like a blackbody. If small grains dominate the emission then the offset is likely to be greater as such grains are inefficient emitters of radiation and thus heat up to higher temperatures at greater distances from the star than would be assumed from a blackbody approximation (see e.g. discussion in Section 3 of Smith & Wyatt 2010).

For two sources not yet discussed we have apparent excess at 8μm with no excess indicated in the other IRAC bands. JC05_472 has a significant excess at 8μm, with $K_s-[8.0] = 0.693\pm0.052$. Other sources of similar colour ($3.8 < V-K_s < 4.8$) have a much lower average $K_s-[8.0] = 0.210\pm0.095$. Although this source lies close to tile edges in the IRAC channel 4 mosaic there is no evidence of the high standard deviation between exposures seen for JC06_240, and thus there is no evidence that the errors have been underestimated. We therefore conclude that there is evidence for an 8μm excess around this target. Unfortunately this source has a low level detection at 24μm ($< 4\sigma$). If we accept the low signal to noise detection as a true reflection of the 24μm flux of the target then the flux (164$\pm$43 mJy) is close to the expected level of flux from this source at 24μm from an SED fit using a Kurucz profile at the temperature taken from Jeffries et al. (2009) and scaled to the 2MASS JHK_s photometry (expected 116mJy from the photosphere). Similarly P155 has a large 8μm excess ($K_s-[8.0] = 0.273\pm0.043$ compared to an average of $0.055\pm$ 0.052 for sources with $V-K_s = 2.3\pm0.5$). This sources falls at the very edge of the mosaiced 24μm image which is dominated by noise and therefore we cannot detect this target nor can we determine limits for its 24μm flux. There are no sources near P155 that could be contaminating the 8μm flux nor are there any indications of high variation between different exposures including this target. For both targets, with no excess at shorter wavelengths and no significant detection at 24μm the nature of the excess emission at 8μm remains currently unresolved.

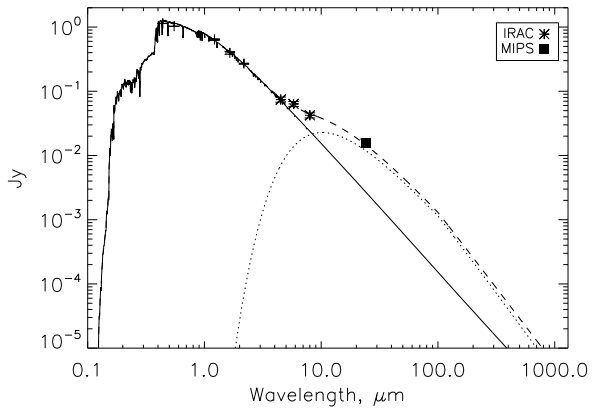

Figure 4. The SED of source TYC424-473-1. A Kurucz profile of 8337K has been scaled to the 2MASS JHK photometry. Overplotted is a blackbody at 500K (dotted line) and the total flux from the photospheric model and blackbody (dashed line). This profile fits the IRAC (asterisks) and MIPS (square) data we have obtained.

4.1.5 Summary

SED plots are constructed for the other targets in our survey in the same way, adopting a temperature as listed in Tables 1 and 2 scaled to the 2MASS JHK photometry of the targets. These were examined for evidence of near-infrared excess and with the exception of the unresolved 8μm issues for JC05_472 and P155 (discussed above), and the excess around TYC424-473-1, none was found. We also compare the targets that appear to have 24μm excess in the SED fit to those that appear to have an excess in the $K_s-[24]$ colour plot (Figure 2). For all such targets the SED is consistent with there being excess emission at 24μm.

In summary one target, TYC424-473-1, has strong evidence of near-infrared excess in all unsaturated observations. For the solar-type JC05_472 and P155 there is some evidence of an 8μm excess (at 5 and 4σ significance respectively) but not of an excess at 24μm or in other IRAC channels. For all other targets with uncontaminated photometry the IRAC photometry is consistent with photospheric emission within the errors (any excess has $< 3\sigma$ significance). The lack of IRAC excess indicates we do not have a population of primordial discs in the sample, as expected at an age of 27Myr. These discs are also unlikely to be transition discs, as the lifetime of such discs is expected to be very short ($\sim$0.3Myr, Skrutskie et al. 1990) and we do not see a remnant primor-

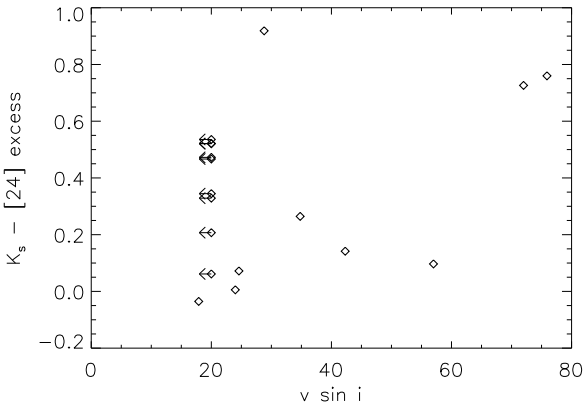

Figure 5. The $K_s - [24]$ excess versus projected rotational velocity for the targets from Jeffries et al. (2009). Here excess is defined by by difference from the photospheric colours determined by Plavchan et al. (2009) as shown in Figure 2. We find no evidence for a relationship between excess and rotational velocity.

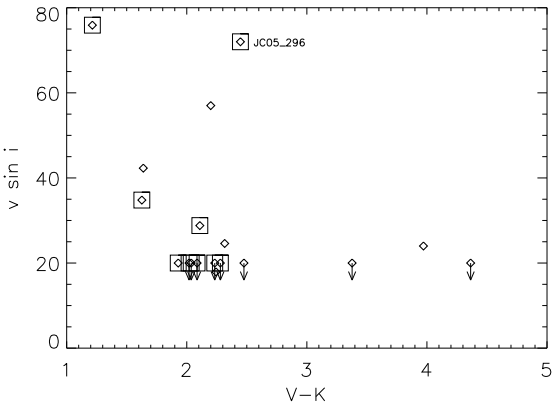

Figure 6. The rotational velocity for the targets from Jeffries et al. (2009) shown by colour. Squares indicate sources which have been judged to have 24μm excess using Figure 2. One K dwarf, JC05_296 (labelled), has a high rotational velocity for its spectral type and apparent 24μm excess. This contradicts the expectations of the wind scouring model of Chen et al. (2005) and Plavchan et al. (2009).

dial disc population. Thus we consider that the 24μm excess is indicative of a debris disc population.

4.2 Link with rotational velocity

Following the study by Stauffer et al. (2010) we search for a link between rotational velocity and the 24μm excess. Stellar winds from low mass stars are thought to be powered by dynamo activity driven by differential rotation. Thus rotational velocity could be used as a proxy for stellar wind. Stellar winds are expected to remove small particles from discs (Chen et al. 2005; Plavchan et al. 2009) and so we might expect a correlation between rotational velocity and 24μm excess. This would not be a linear relation as the stellar wind is believed to saturate above some rotational velocity. Figure 5 shows the rotational velocity of the targets from Jeffries et al. (2009) versus infrared excess as measured by the difference between the photospheric relation given by Plavchan et al. (2009) (solid line, Figure 2) and the measured $K_s - [24]$. This can be compared directly with Figure 7 of Stauffer et al. (2010). We have no rotational velocity information for the Tycho targets in our survey, and the two sources included from Prosser & Giampapa (1994) have badly contaminated and thus unreliable 24μm photometry.

For many of our targets the measurements of Jeffries et al. (2009) provide only upper limits to the rotational velocity of the targets (indicated by arrows in Figure 5). Accepting this limitation, there is no evidence in the figure for a decrease in excess with increased rotational velocity. A similar null result was reported in Stauffer et al. (2010), who argued that this result does not suggest that the wind scouring model is incorrect as the sample mostly shows the expected relation between rotational velocity and colour (lower mass stars such as late F and G dwarfs are expected to be slow rotators, early F type stars are rapid rotators). Within their sample only one rapidly rotating lower mass target was found which has no excess emission, and therefore the Stauffer et al. (2010) sample could not be used to constrain the wind scouring model. If we examine our targets in a similar way we find one rapidly rotating K dwarf with an excess, as shown in Figure 6. This star is JC05_296, a target with an excess in $K_s - [24]$ of 0.794±0.161. As we have only one such target and suffer from small number statistics we cannot draw significant conclusions on the validity of the wind scouring model based on our results. Further work in this area to obtain a large enough sample to test the model on a statistical basis is required.

4.3 Link with multiplicity

Cieza et al. (2009) presented evidence for the impact of stellar multiplicity on the evolution of circumstellar discs. Using the IRAC data from several Spitzer legacy surveys they found that for projected separations of <40AU systems were half as likely to retain their primordial discs than systems with larger separations (suggesting a disc lifetime of 0.3-0.5Myr for close binaries compared to 3-5Myr around single stars). Conversely Trilling et al. (2007) found no evidence for a link between debris disc detection and binarity in their study of field stars (with most stars >600Myr old). This survey concentrated on detections at 70μm, and so on discs that were further from their host stars. Plavchan et al. (2009) found no evidence of the trend suggested by Trilling et al. (2007), and Duchêne (2010) found no significant dependence of debris disc incidence with binarity or binary separation. Stauffer et al. (2010) showed tentative evidence that in the 100Myr Blanco 1 cluster there is a link between 24μm excess and binarity (or rather with a binarity proxy). They combine their results with data from the Pleiades ($\sim$ 100Myr) and NGC2547 ($\sim$ 30Myr) and find an overall chance of 0.05% that the excess around single and binary samples is drawn from the same parent population (using a K-S test). We follow their example and use height above a single star isochrone as a proxy for binarity and compare this to the $K_s - [24]$ excess. The isochrone was tuned from a fit to

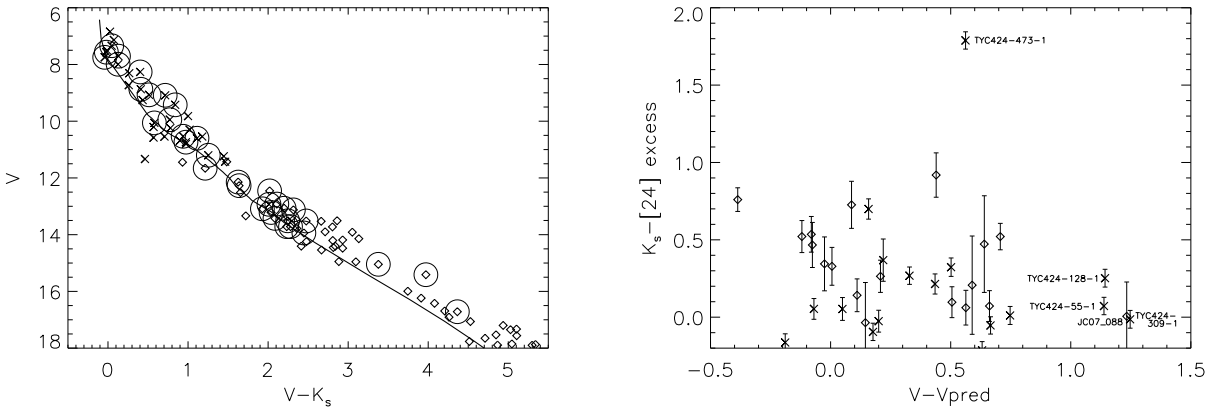

Figure 7. Dependence of excess on a proxy for multiplicity. We use height above the single star isochrone (left) as a proxy for binarity following Stauffer et al. (2010). The diamonds and crosses in both plots indicate targets from Jeffries et al. (2009) and those listed in Table 2 respectively. Stars with good (signal to noise >5) 24μm detections are indicated by circles. We find no evidence for a link between excess and binarity (right).

the Pleiades following Stauffer et al. (2007). The results are shown in Figure 7.

Four targets have $V - V_{\rm pred}$ much higher than would indicate a binary system (0.75 for an equal mass binary, where $V_{\rm pred}$ is the predicted value of V for a given value of $V - K_s$ using the single star isochrone). If these stars have higher multiplicity (triple or higher order systems) then of our 35 high signal to noise detections we would have a 11^{+9}_{-5}% detection of triple or higher order systems. This is compatible with previous studies (see e.g. Abt 1983, Abt & Levy 1976). One of these systems, TYC424-128-1, has significant excess at 24μm. In general we find no significant evidence for a dependence of excess on height above the isochrone. Separating the sample into those with a height above the single star isochrone of $\geqslant 0.3$ (in V) and those below this level a K-S test returns a 32% probability that the two populations are drawn from the same parent distribution. The star with the highest $K_s - [24]$ is TYC424-473-1, the star which also has a near-infrared excess. The value of $V - Vpred$ found for this target (0.59) suggests that this star is a binary and the two components are likely to be close in mass. Using this value to constrain our SED fitting we find a fit with a secondary component could have a temperature of 7590K (suggesting spectral types of A4V for the major component and A8V for the companion). This does not affect the fit to the excess emission presented in section 4.1.

Amongst the sources taken from Jeffries et al. (2009) there are two targets with significant excess in $K_s - [24]$ that are likely binaries (JC02_373, $V - Vpred = 0.71$, $K_s - [24] = 0.52 \pm 0.09$; JC08_257, $V - Vpred = 0.44$, $K_s - [24] = 0.92 \pm 0.14$). These two sources suggest that in this system the multiplicity of the star has no influence on the presence of a debris disc. In the cluster samples considered by Stauffer et al. (2010) there is one large excess around a likely binary in the Pleiades. As we are dealing with small number statistics these examples do not represent a significant contradiction of the finding that binary and single stars have different debris disc populations. However, we find no significant evidence for such a dependence in the IC4665 cluster.

5 PLACING IC 4665 INTO CONTEXT

Following the examples of Siegler et al. (2007) and Meyer et al. (2008) we add the results from the IC 4665 cluster to the growing sample of solar-type stars studied with MIPS. These studies and references are listed in Table 4. Sources included in the table are of spectral type F5-K5. This range covers the solar-type stars that are bright enough to have their photospheres detected at a signal to noise of at least 3 in our MIPS 24μm imaging. For a 3σ detection in the MIPS 24μm image a source is required to have a magnitude of $[24] \leqslant 11.8$. This means we are complete to $\sim$K5. Concentrating on F5-K5 type stars ($1.3 \geqslant V - K_s \leqslant 3.05$) gives us a sample of 25 stars in the MIPS field. If we consider only the sample restricted to this limit our excess detection rate becomes 10/24 or 42^{+18}_{-13}%. This is somewhat higher than other samples of a similar age, but not significantly so (see Table 4). Compared to the FEPS targets presented in Meyer et al. (2008), in which the frequency of 24μm excess was found to be $0.19^{+0.09}_{-0.06}$ for stars aged 10-30Myr and $0.08^{+0.06}_{-0.04}$ for stars aged 30-100Myr, IC 4665 has a reasonably large fraction of sources with debris disc emission at 24um. We show the frequency of 24μm excess in the samples listed in Table 4 and the Meyer et al. (2008) sample in Figure 9. Note that a uniform detection threshold ($F_{24}/F_{\rm phot} = 1.15$) is used in all these surveys with the exception of the Pleiades cluster (Sierchio et al. 2010). For this cluster we also show the frequency in the case that the higher threshold is used. The detection threshold used for the IC4665 cluster (as given by the error calculation in section 4) is higher than this limit for the lower mass stars considered, however examination of Figure 2 indicates that there are no objects in the region between the statistical errors shown and a limit of $F_{24}/F_{\rm phot} = 1.15$, and thus we consider that these results are compatible with the other cluster samples. The same spectral range (F5-K5) is considered for all clusters (and so the excess frequency may differ to those quoted in the papers, and in Siegler et al. 2007, where they consider a different spectral range.) In this plot we can see that the overall frequency of excess emission in IC 4665 is the highest of the

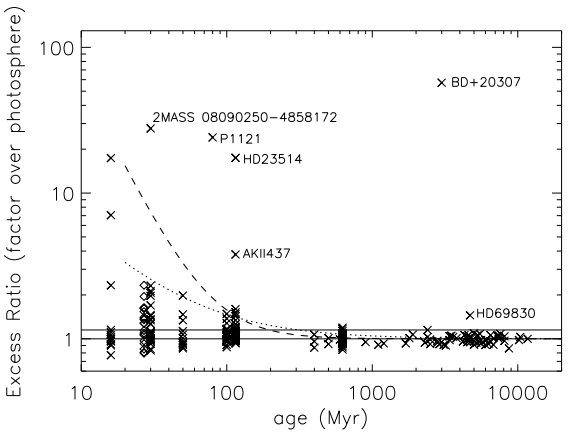

Figure 8. The 24μm excess emission around stars in the studies listed in Table 4. The sources from this paper are marked with diamonds. Sources with high excess compared to typical ranges for their age are named. In addition to the cluster data listed in Table 4 we show BD+20307 (Song et al. 2005, **age several Gyr from Zuckerman et al. 2008**) and P1121 in M47 (Gorlova et al. 2006). Overplotted are an inverse time dependence (dotted line) and an inverse time-squared dependence (dashed line).

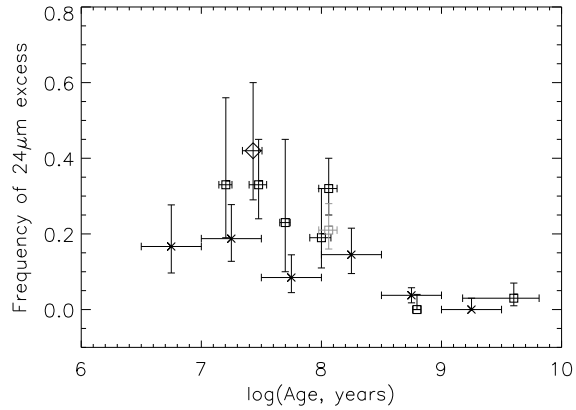

Figure 9. The frequency of 24μm excess emission in the samples listed in Table 4 (squares) and in the Meyer et al. (2008) sample (crosses). The IC 4665 cluster data presented in this paper is marked with a diamond. The grey square marks the excess fraction seen in the Pleiades if we adopt an excess detection level of $F/F* = 1.15$ as is typical for the other samples in the plot (see Table 4.

cluster samples listed in Table 4 but within the errors is consistent with the frequencies seen in other clusters of similar ages.

In Figure 8 we show the level of 24μm excess (expressed as measured flux over that expected from the photosphere) seen in studies of different clusters. Overplotted are an inverse time and an inverse time-squared dependence. As first suggested by Siegler et al. (2007), the inverse time-squared dependence seems to offer the best fit to the upper envelope of excess for the Upper Scorpious and Lower Centaurus Crux members of the Scorpius-Centaurus association (data from Chen et al. 2005), but the inverse time dependence is a better fit to the rest of the data. An inverse time dependence has also been shown to fit A star debris disc statistics (Rieke et al. 2005). This agrees with predictions for steady-state evolution of debris discs, in which the excess emission arising from the debris discs falls inversely in proportion to time. This $time^{-1}$ fall-off arises once the debris reaches a collisional equilibrium in which the largest bodies in the population are colliding and producing smaller material which is eventually collisionally processed into dust small enough to be removed from the system (Dominik & Decin 2003; Wyatt et al. 2007).

Compared to the 30Myr old cluster NGC 2547 the excess levels seen in IC 4665 show a similar spread apart from the presence of one high excess source in NGC 2547, 2MASS 08090250-4858172 (labelled ID 8 in Gorlova et al. 2006; this source has excess emission from 3μm and is possibly a primordial optically thick disc). Our results are consistent with the inverse time dependence. We find no sources that exceed this envelope and could be considered to have dust resulting from a transient event as has been postulated for HD69830 and BD+20307 (Wyatt et al. 2007). Extreme levels of excess could be interpreted as evidence for a recent massive collision such as those expected between protoplanets in the final stages of terrestrial planet accretion (Weidenschilling 1977). Simulations by Kenyon & Bromley (2005) have shown that at an age of 27Myr a collisional cascade in a minimum-mass solar nebula around a solar-type star at 0.4–2AU would be above our detection threshold, and so could be a valid model for the emission we detect. Similarly around higher mass stars the emission could arise from a collisional cascade at 3–20AU or 30–150AU. With a single photometric detection for most of these targets we cannot constrain either the location or the mass of the dust, however these models show that a collisional cascade produced by catastrophic collisions in a disc is a possible model for the emission seen here.

We can also consider the relative proportions of different levels of excess in the clusters studied. We follow the example set by Rieke et al. (2005) who showed the rates of low, intermediate and high excess fractions as a function of time to explore the decay of debris discs around A stars. We split the samples for each cluster into small or no excess ($F_{24}/F_{\rm phot} < 1.25$, where $F_{\rm phot}$ is the expected flux from the stellar photosphere), intermediate excess ($1.25 < F_{24}/F_{\rm phot} < 2.$), and large excess ($F_{24}/F_{\rm phot} > 2$). These are plotted as a function of age in Figure 10. The general pattern of excess is similar to that seen around A stars, with the proportion of targets having low or no excess ($F_{24}/F_{\rm phot} < 1.25$) increasing with age, and the proportion of sources with intermediate excess being higher than those with large excess ($F_{24}/F_{\rm phot} > 2$) for all but the youngest sub-sample (compare with Figure 3 of Rieke et al. 2005 and Figure 9 of Su et al. 2006). This suggests that the evolution of debris around both solar-type stars and more massive stars follows a similar pattern, although the timescale is an order of magnitude longer for more massive stars (see Figure 6 of Siegler et al. 2007).

We can also see in Figure 10 that IC 4665 and NGC 4547 which are of the similar age appear to have somewhat different distributions. A higher proportion of the sources in IC 4665 have intermediate levels of excess ($1.25 < F_{24}/F_{\rm phot} < 2$) than for any other cluster (although not significantly so). Consequently the proportion of sources with no or low

Table 4. Frequency of 24μm excess from cluster data (after Siegler et al. 2007)

Name	Age, Myr	Number of sources	Excess frequency	Reference
Sco Cen	16±2	15	$0.33^{+0.23}_{-0.14}$	Chen et al. (2005)
IC 4665	**27±5**	**24**	$\mathbf{0.42}^{+0.18}_{-0.13}$	**This paper**
NGC 2547	30±5	39	$0.33^{+0.13}_{-0.09}$	Gorlova et al. (2007)
IC 2391	50±5	13	$0.23^{+0.22}_{-0.13}$	Siegler et al. (2007)
Blanco 1	100±20	26	$0.19^{+0.13}_{-0.08}$	Stauffer et al. (2010)
Pleiades	115±20	71	$0.32^{+0.08}_{-0.07}{}^{a}$	Sierchio et al. (2010)
Hyades	625±50	63	0.00±0.04	Cieza et al. (2008)
Field stars	$\sim$4000[b]	69	$0.03^{+0.04}_{-0.02}$	Bryden et al. (2006)

[a] Uses an excess detection threshold of 1.10. Majority of other surveys use a threshold of 1.15 (if adopting this higher threshold excess frequency becomes $0.21^{+0.07}_{-0.05}$).
[b] Median age of the sample

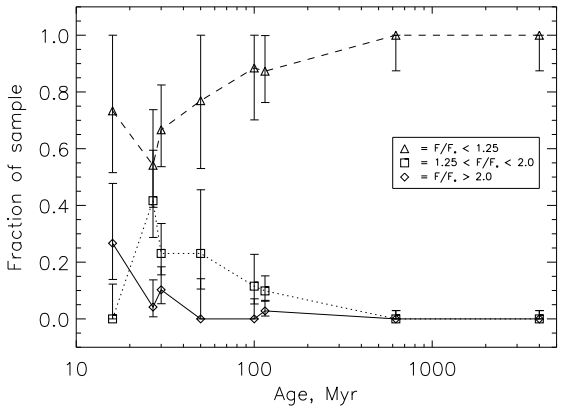

Figure 10. Fraction of stars with low or no excess ($F_{24}/F_{\rm phot} < 1.25$), intermediate excess ($1.25 < F_{24}/F_{\rm phot} < 2$) and high excess ($F_{24}/F_{\rm phot} > 2$) for each of the cluster samples listed in Table 4. The overall trend agrees well with the A stars as shown in Figure 3 of Rieke et al. (2005) and Figure 9 of Su et al. (2006). The distribution of excess for the IC 4665 cluster presented in this paper (shown at 27 Myr) is somewhat different from the other cluster of a similar age, NGC 2547.

excess ($F_{24}/F_{\rm phot} < 1.25$) is lower than the other published clusters (again not significantly so). If assume that the minimum mass solar nebula (MMSN) predictions from Kenyon & Bromley (2005) for the evolution of debris in the final stages of terrestrial planet formation can be applied to our cluster data, then the frequency of discs with intermediate excess in IC 4665 would suggest that many stars in the cluster have recently experienced a large collision. However, as the initial planetesimal discs may have differed from a MMSN then we cannot confirm this is the case.

To further test whether the distribution of excess emission in IC 4665 is different to other sources we examine the cumulative distribution functions of the excess emission of each cluster. The resulting normalised distributions are shown in Figure 11. As we can see here the older clusters and the field have very similar distribution functions, which are somewhat different to the younger sources shown in the left-hand plot. This is to be expected if the evolutionary timescale for debris discs is of the order of 10-100Myr. The cumulative frequency (CF) distribution for IC 4665 has some differences to the CF distribution of NGC 2547, however a two-sample Kolmogorov-Smirnov (K-S) test indicates that the probability that the two cluster samples are drawn from the same underlying probability distribution is still 76%. The probability that the IC 4665 and Sco Cen samples are drawn from the same distribution is 26%. This is not low enough to confirm a significant difference between the clusters, although the CF distribution looks quite different. There is evidence that the underlying distribution could be different for the older samples. A K-S test comparing IC 4665 to these samples returns a probability that the underlying distributions are the same of 8% (Blanco 1, 100Myr), 1% (Pleiades, 115Myr), 0.04% (Hyades, 625Myr) and 0.02% (field sample, average age 4000Myr). This provides further support for evolution of debris discs on 10-100Myr timescales.

We find no evidence of a link between binarity and excess seen in IC 4665. A binary companion limits the size of a stable region for a circumbinary disc to $\leqslant a_{\rm crit}$, a function of the binary's configuration (e.g. Holman & Wiegert 1999). This limit also approximately corresponds to the region in which the final chaotic stages of planet formation from lunar-sized embryos can proceed (Quintana et al. 2007). This truncation of planet formation in binaries is of particular interest given the recent discoveries of $\sim$ 80 exoplanets in binary systems (see e.g. Desidera & Barbieri 2007, Mugrauer & Neuhüser 2009). The presence of dust grains in so-called forbidden regions ($< a_{\rm crit}$) found for several binary systems by Trilling et al. (2007) may be explained by recent numerical simulations in Thèbault et al. (2010) who found that small grains can populate the forbidden region. The amount of dust in unstable regions depends on the balance between the rate of small grain production through collisions and removal by the perturbations of the binary. As discussed in section 4.3 several studies have offered contradictory evidence for a link between multiplicity and the presence of a debris disc (Cieza et al. 2009; Trilling et al. 2007; Stauffer et al. 2010). With the wealth of seemingly contradictory conclusions about the relationship between binarity and debris disc incidence further studies, in particular exploring the geometry of the binary system and the true dust distributions to remove degeneracies from SED fitting, are needed. For example the two likely binary sources in IC4665

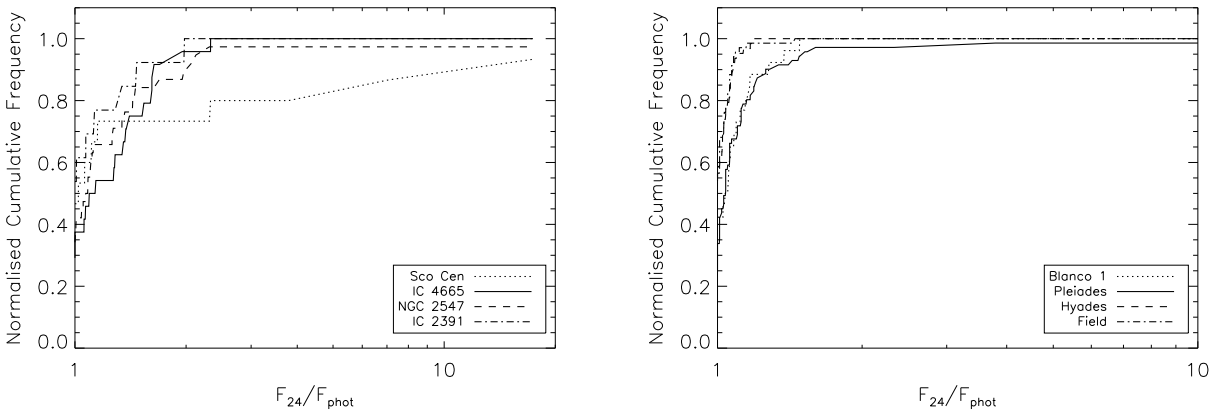

Figure 11. The normalised cumulative frequency distributions of the excess emission for the clusters listed in Table 4. The younger clusters are shown in the left-hand plot and the older clusters ($\geqslant$ 100Myr) in the right-hand plot. The distribution of IC 4665 (solid line, left-hand plot) could be drawn from the same underlying distribution as the other sources $\leqslant$ 50Myr (shown in the left-hand plot), but is unlikely to be drawn from the same distribution of excesses as the older clusters (see text for details).

with significant excess (JC02_373 and JC08_257) could be wide binaries (several hundered AU) which would not be resolved in the Spitzer observations and would not be expected to affect the presence of 24μm excess.

6 CONCLUSIONS

In this paper we have presented a study of the cluster IC 4665 using Spitzer IRAC and MIPS data. These data have been used to search for debris discs in the cluster. Our conclusions are:

- the cluster IC 4665 has the highest incidence of 24μm excess in the spectral range F5-K5 of all the clusters studied with Spitzer to date, although the rate (42^{+18}_{-13}%) is not significantly higher than the similarly aged NGC 2547 (33^{+13}_{-9}%). The majority of the sources in the cluster have low or intermediate levels of excess $F_{24}/F_{\rm phot} < 2$. No sources in IC 4665 have excess above the levels expected for an inverse time decay of debris predicted by collisional evolution models;
- the source TYC424-473-1, which may be a binary, has excess in all unsaturated observations indicative of excess emission from the near to mid-infrared. Such near-infrared excess could indicate the presence of a remnant primordial disc. This excess can be fit by a simple blackbody curve at a temperature of 500K suggesting a radial offset of $\sim$1.7AU from the star;
- there is no evidence of a dependence of excess at 24μm on multiplicity of the star in this cluster. We find several sources which are suspected multiples that have significant 24μm excess, but as the numbers are small these do not provide contradictory evidence against the recent work by Stauffer et al. (2010) who found evidence that 24μm excess is reduced around multiple stars in other clusters. More work to explore the nature of the multiple stars, in particular to determine the system geometry and the location and distribution of dusty debris in these systems is necessary to determine the nature of any link between excess and multiplicity.

ACKNOWLEDGMENTS

REFERENCES

Abt H.A., Levy S.G., 1976, ApJS, 30, 273
Abt H.A., 1983, ARA&A, 21, 343
Backman D.E., Paresce F., 1993, in Protostars and Planets III, ed. E.H. Levy, J.I. Lunine (Tuscon:University of Arizona Press), 1253
Baraffe I., Chabrier G., Allard F., Hauschildt P.H., 2002, A&A, 382, 563
Bessell M.S., Castelli F., Plez B., 1998, A&A, 333, 231
Bryden G., et al., 2006, ApJ, 636, 1098
Carpenter J.M., Mamajek E.E., Hillenbrand L.A., Meyer, M.R., 2009, ApJ, 705, 1671
Canup, R.M., 2004, ARA&A, 42, 441
Chambers, J.E., 2001, Icarus, 152, 205
Chen, C.H., Jura, M., Gordon, K.D., Blaylock, M., 2005, ApJ, 623, 493
Cieza L.A., Cochran W.D., Augereau J-C., 2008, ApJ, 679, 720
Cieza L.A., et al., 2009, ApJ, 696, L84
Crawford D.L., Barnes J.V., 1972, AJ, 77, 862
Desidera S., Babieri M., 2007, A&A, 462, 345
Dominik C., Decin G., 2003, ApJ, 598, 626
Duchêne G., 2010, ApJ, 709, L114
Engelbracht C.W., et. al., 2007, PASP, 119, 994
Fazio G.G., et. al., 2004, ApJSS, 154, 10
Gorlova N., et. al., 2006, ApJ, 649, 1028
Gorlova N., et. al., 2007, ApJ, 670, 516
Høg E., et al., 2000, The Tycho-2 catalogue of the 2.5 million brightest stars
Holman M.J., Wiegert P.A., 1999, AJ, 117, 621
Hogg A.R., Kron G.E., 1955, AJ, 60, 365
Jeffries R.D., Jackson R.J., James D.J., Cargile P.A., 2009, MNRAS, 400, 317
Kenyon S.J., Bromley B.C., 2005, AJ, 130, 269
Kenyon S.J., Bromley B.C., 2006, AJ, 131, 1837
Kenyon S.J., Hartmann L., 1995, ApJS, 101, 117
Klahr H., 2008, NewAR, 52, 78
Lagrange A.M., Backman D.E., Artymowicz P., 2000, in

Protostars and Planets IV, ed. V Mannings, AP Boss, SS Russell, (Tuscon:University of Arizona Press) 639
Lisse C.M., et al., 2009, ApJ, 701, 2019
Mamajek E.E., 2007, IAU Symposium, 437, 442
Manzi S., Randich S., de Wit, W.J., Palla F., 2008, A&A, 479, 141
Makovoz D., Marleau F., 2005, PASP, 117, 1113
Meyer M.R., et al., 2008, ApJ, 673, L181
Mugrauer M., Neuhüser R., 2009, A&A, 494, 373
Plavchan P., et al., 2009, ApJ, 698, 1068
Prosser C.F., Giampapa M.S., AJ, 1994, 108, 964
Quintana E.V., Adams F.C., Lissauer J.J., Chambers J.E., 2007, ApJ, 660, 807
Reach W.T., et al., 2005, PASP, 117, 978
Rebull L.M., et al., 2008, ApJ, 681, 1484
Rieke G.H., et al., 2004, ApJS, 154, 25
Rieke G.H., et al., 2005, ApJ, 620, 1010
Siegler N., et al., 2007, ApJ, 654, 580
Sierchio J.M., et al., 2010, ApJ, 712, 1421
Siess L., Dufour E., Forestini M., 2000, A&A, 358, 593
Skrutskie M.F., et al., 1990, AJ, 99, 1187
Skrutskie M.F., et al., 2006, The Two Micron All Sky Survey (2MASS)
Smith R., Wyatt M.C, 2010, A&A, 515, 95
Song I., Zuckerman B., Weinberger A.J., Becklin E.E., 2005, Nature, 436, 363
Stauffer J.R., et al., 2010, ApJ accepted, arXiv:1007.0239
Stauffer J.R., et al., 2007, ApJS, 172, 663
Su K.Y.L., et al., 2006, ApJ, 653, 675
Thèbault, P., Marzari F., Augereau J.-C., 2010, A&A accepted, arXiv1008.1264
Trilling, D.E., et al., 2007, ApJ, 658, 1289
Weidenschilling S.J., 1977, MNRAS, 180, 57
Weidenschilling S.J., Cuzzi J.N., 1993, in Protostars and Planets III, ed. E.H. Levy, J.I. Lunine (Tuscon:University of Arizona Press), 1031
Wyatt M.C., 2008, ARAA, 46, 339
Wyatt M.C., et al. 2007, ApJ, 658, 569
Zacharias N., Monet D.G., Levine S.E., Urban S.E., Gaume R., Wycoff G.L., 2005, NOMAD Catalog
Zuckerman B., et al. 2008, ApJ, 688, 1345

This paper has been typeset from a TEX/ LATEX file prepared by the author.